SCIENTIFIC Publishing Limited

Journal of Infectious Diseases and Public Health

https://ojs.ukscip.com/index.php/jidph

Article

Deep Learning-Based Detection of Aseptic Meningitis Using CNN and K-Means Clustering

Syed Shahid Shah [1,*], Mansoor Ahmad [2], and Sajjad Ahmad [3]

[1] School of Electronics & Information Engineering, Beihang University, Beijing 100191, China

[2] Department of Electrical Engineering, University of Engineering and Technology, Peshawar 25120, Pakistan

[3] School of Mathematical Sciences, Bahauddin Zakariya University, Multan 60800, Pakistan

[*] Correspondence: eng.shahid@buaa.edu.cn

Received: 2 September 2025; **Revised:** 11 October 2025; **Accepted:** 21 October 2025; **Published:** 28 October 2025

Abstract: Aseptic meningitis is a serious neurological disorder that poses diagnostic challenges due to overlapping symptoms with other conditions and the limitations of conventional diagnostic techniques. Existing approaches often rely on invasive procedures or subjective interpretation of medical images, leading to delays or misdiagnosis. The condition leads to high mortality, especially amongst individuals with Human Immunodeficiency Virus (HIV), and predicting the incidence of disease-related complications remains challenging, with the value of brain magnetic resonance imaging (MRI) not yet fully explored. To address this, we used a convolutional neural network (CNN) to investigate the complementary contribution of brain MRI to conventional prognostic determinants. A hybrid approach was developed, integrating CNN-based autonomous feature extraction and recognition with K-Means clustering for efficient segmentation of medical images. Quantitatively, the proposed model achieved a test AUC of 84.1% ± 2.6, accuracy of 81.3% ± 2.7, F1-score of 79.2% ± 2.4, and balanced accuracy of 77.3% ± 2.3, consistently outperforming ResNet50, DenseNet121, U-Net, Vision Transformer, and Swin-UNet across all evaluation metrics. The framework offers a fast, accurate, and non-invasive decision-support tool designed to assist clinicians in the timely identification and management of aseptic meningitis, ultimately improving patient care and outcomes.

Keywords: Aseptic Meningitis; Image Processing; Deep Neural Network; Convolutional Neural Network; MRI; Feature Extraction; Clustering; K-Means

1. Introduction

Aseptic meningitis is an inflammatory neurological disorder characterized by meningeal irritation in the absence of detectable bacterial infection in cerebrospinal fluid cultures. It is among the most widely recognized, typically generous, fiery problems of the tissues. Viral infections are a specific cause; however, there are also numerous additional infectious and non-infectious factors [1]. In this way, the terms meningitis, infectious, and viral meningitis cannot be substituted. Symptoms may vary based on the type; Manifestations can change according to the etiology and the status of the host. Patients with insufficient humoral resistance are at a higher risk of negative results, including children and patients with agammaglobulinemia [2]. The etiology of aseptic meningitis is divided into infectious and non-infectious agents. The infectious causes include infections, growths, and parasites, while the non-infectious causes include post-contamination irritation, drugs, underlying infections, and neoplastic problems [3]. The reason can at last simply be distinguished in 30% to 65% of the cases. The most common reason is viral, most often enteroviruses, followed by herpes simplex infection and varicella-zoster. Aseptic Meningitis is a

disease characterized by extreme inflammation of the meninges, typically accompanied by mononuclear pleocytosis. Clinical indications change, with migraine and fever prevailing.

The disease is generally self-limiting; however, severe neurological complications may occur in certain patient populations [4]. Digital image processing involves using computer algorithms to process a digital image to obtain an enhanced image by gathering useful information. The fragmentation of a picture into various areas with pixels of the same attributes is the segmentation of an image [5]. It makes the examination simpler and interprets the picture. In the medical field, image processing methods, including Computed Tomography (CT), Positron Emission Tomography (PET), and MRI, are widely applied to diagnose brain diseases. By comparing all these techniques, MRI delivers precise pictures of the central nervous system since it can produce images with high resolution, because of its superior soft tissue contrast in humans [6].

For many years, image processing has been practiced. Every year, a slew of new techniques and technologies are developed to handle image processing problems [7]. Due to the vast amount of data to be processed, image processing is typically performed by a computer. This is due to the fact that each color must be identified to enable computer processing, as well as a contemporary image may include over 200 million colors. Only a supercomputer, on the other hand, can genuinely process a fully colored image [8]. For ease of processing, several codes turn the picture into black and white. The majority of algorithms struggle to analyze images in a noisy environment [9]. When creating an image processing system, edge detection is one of the most commonly employed techniques. This is because the edge of an item is the easiest thing to see in human perception [10]. The techniques of analyzing medical images for identifying neurological abnormalities have significantly advanced due to the rapid development of artificial intelligence and deep learning algorithms [11]. Alzheimer's disease, encephalitis, cancers of the brain, and inflammatory infections of the central nervous system are merely some of the neurological conditions for which MRI-based automated diagnostic techniques have displayed considerable promise in the past decade [12]. Architectural imaging characteristics can be directly determined from MRI scans by employing deep learning algorithms, especially CNN, which overcomes the necessity for human feature engineering [13]. CNN-based approaches provide better precision and resilience for objectives like lesion localization, segmentation, as well as medical picture classification, as reported in current studies [14]. Strategies involving shape analysis, texture representation, and automated feature extraction have been highly beneficial for recognizing structural anomalies in MRI-based neurological illnesses [15].

Moreover, standard approaches to segmentation that incorporate deep learning frameworks with conventional clustering techniques display substantial prospects for discovering irregular anatomical sections and lowering structural diversity based on neuroimaging results [16]. Due in a significant way to being able to obtain both local and global contextual information, transformer-based configurations are now becoming a successful replacement for MRI segmentation along with disease localization [17]. In convoluted biological scenarios, hybrid learning systems that merge CNN with clustering algorithms have also shown greater prediction precision, superior feature localization, and stronger classification efficiency [18]. To determine common structural trends in medical images, a number of articles focused on texture analysis and region-based feature extraction strategies [19]. By boosting contrasting variability and suppressing noise artefacts, innovative image modification and segmentation methodologies have substantially facilitated the identification of abnormal sites in MRI scans [20].

In automated technology testing situations and virtual medical facilities, deep learning algorithms in combination with specialized image processing algorithms have established enormous possibilities for autonomous infectious disease assessment [21]. Likewise, advances in adaptive healthcare facilities and environmentally friendly computation facilities have allowed the large-scale application of deep learning technologies in medical imaging purposes [22]. Several studies have additionally explored disease severity estimation and lesion quantification using image processing and deep learning methodologies [23]. Automated detection frameworks utilizing MRI preprocessing, segmentation, and structural feature analysis have demonstrated substantial promise in improving neurological disease diagnosis and prognostic assessment [24].

To identify abnormal tissue regions and structural neurological changes, computational imaging techniques integrated with machine learning and deep learning algorithms have increasingly been employed in modern medical imaging systems [25]. An employed neural network with a feed-forward function that is not restricted to 2D pictures. CNN draws inspiration from physiological functions [26]; Relying upon the identical balancing design along with translational permanence, CNNs are classified as either space or delayed determinants, in contrast to other

types of neural network designs [27]. Recent advancements in artificial intelligence and computational medical imaging have enabled the generation and analysis of large-scale biomedical data for disease diagnosis and prognostic assessment. The efficient application of CNN in biotechnology primarily addresses problems like the categorization and division of scientific pictures [28–31], employed in the nervous system malignancy [32], thyroid [33], sperm [34], and pulmonary artery [35,36]. In addition, CNNs are also used to address issues such as genome sequencing, RNA and DNA analysis [37,38], and protein structure analysis [39], and to analyze respiratory data to detect chronic and non-chronic diseases [40]. K-means is a clustering algorithm, whereby a certain set of data is fixed in advance, classified into k disjoint clusters. The algorithm consists of two distinct phases, each of which is to define k centroids. The next phase involves the identification and association of each piece of information throughout the collection with the closest centroid [41].

Cluster analysis is one of the major methods of data analysis used for many practical purposes in emerging fields, such as Bioinformatics. K-means is an effective algorithm for producing clusters in many useful applications [42]. With the increasing advancement in the medical field, including brain tumour [43], heart disease, skin problems, hippocampus, and Alzheimer's [44]. In order to assess the predictive usefulness of clinical and imaging characteristics for aseptic meningitis outcomes, this study examined a cohort of 215 patients with an incidence of 22.3%. The non-imaging model outperformed the imaging-only model on the test set, while the fused model, which combined the two feature types, achieved the highest average AUC. According to the findings, imaging features contributed more to predictions in HIV-negative patients, while non-imaging variables were more useful in HIV-positive individuals.

2. Methodology

In order to predict potential neurological ailments from brain MRI data, CNN and K-means clustering are merged in the system. Mechanical characteristic extraction and image segmentation are the two functionalities of this implementation. The information being provided, MRI data, is first processed using K-means clustering. It facilitates distinguishing between essential physiological areas by classifying pixels according to luminosity similarity. These locations involve the cardiovascular system, intracranial spaces, and central meninges, which often display irregularities in brain disorders. At this point, neither direct annotation nor preliminary labelling is mandatory. The partitioned regions undergo further processing by the CNN. Differentiating image features is immediately learned by network algorithms from the information. Conversely, with usual procedures, customized feature development is not required. The CNN is used to determine patterns associated with structural shifts due to disorders, among them basal augmentation, hydrocephalus, and vasculitis. In addition, the two strategies are beneficial. Prospective segments of concern are localized employing K-means clustering. After that, CNN makes use of learnt characteristics for classifying corresponding areas. Overall, feature localization and classification efficiency are boosted by this two-step procedure. As a consequence, brain MRI scans may be examined accurately and independently. In general, by precisely recognizing disease-related imaging occurrences, the design enables a simple instrument for facilitating clinical diagnosis. The network's fundamental structural revisions are depicted in **Figure 1**. These comprise subarachnoid tissue engagement, hydrocephalus-related ventricular expansion, basal stimulation, and artery wall stiffness from disease.

2.1. Novelty and Integration of CNN with K-Means Clustering

The proposed strategy enables a hybrid convergence of CNN and K-Means clustering for regulated MRI-based diagnosis of aseptic meningitis. In the current research, K-Means clustering is implemented as a supplementary categorization and feature-localization methodology that strengthens the CNN feature-learning abilities rather than as an autonomous classifier. First, by dividing MRI scans into homogeneous intensity-focused sections, K-Means clustering provides a process to discard noisy and redundant context information while distinguishing strategically crucial spatial positions. These segments are analyzed via the CNN framework, where structured deep visualizations are automatically obtained from both local and global image structures. According to traditional unilateral deep learning techniques, the combination of CNN and K-Means offers a number of significant benefits. Initially, clustering helps the CNN model concentrate on clinically significant structures linked to neurological disorders and enhances regional consistency. Second, during model training, the segmentation-guided feature extraction method

enhances feature localization and reduces inter-class ambiguity. Third, the approach for assessing neurological complications is more robust and predictive; the suggested fused framework integrates imaging and non-imaging clinical characteristics. The synergistic integration of deep learning and unsupervised clustering within a single MRI-based prognostic system for the automated identification of aseptic meningitis constitutes the core methodological approach of this work.

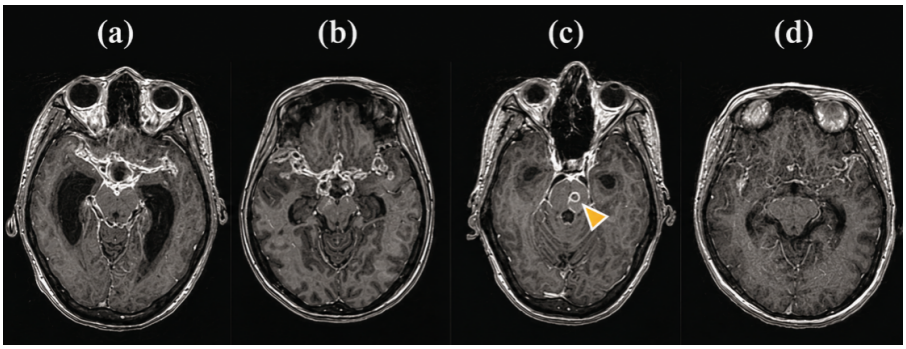

Figure 1. Typical findings on MRI-T1 MPRAGE: (**a**) basal enhancement, vasculitis with thickened vascular walls, and hydrocephalus with dilated lateral ventricles; (**b**) basal enhancement; (**c**) subarachnoid regions (arrow); (**d**) vasculitis.

In order to separate structurally identical tissue regions from unrelated background data, the K-Means clustering component was constructed using Euclidean distance-based partitioning with K = 4 clusters. To enhance clustering stability and convergence efficiency, centroid initialization was carried out using the K-Means++ initialization approach. Until the centroid variation reached a predetermined convergence threshold or the maximum number of iterations was reached, the clustering process was repeatedly optimized. K-Means clustering produced segmented outputs, which were then used as localized structural representations for CNN-based multilevel extraction of features and classification. A neural network design with three main modules was created in order to incorporate imaging data into the prognostic paradigm. To create high-level representations, MRIs were initially handled using an imaging feature extractor made up of 10 convolutional blocks. This was followed by an adaptable average pooling layer and a fully connected (FC) layer. The non-imaging feature extractor was subsequently a different shallow, fully integrated network that was used to extract features from laboratory and clinical parameters. Eventually, the results from the imaging and non-imaging feature extractors were combined and run through a three-layer fully linked classifier. **Figure 2** shows the entire framework of the proposed paradigm.

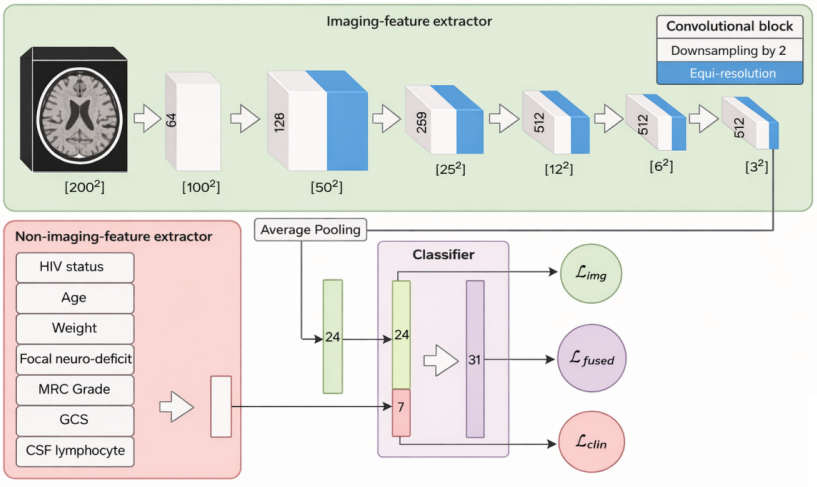

Figure 2. Proposed fused CNN architecture.

The data pretreatment workflow for MRI-based analysis is depicted in the **Figure 3**. Initially, 264 people were taken into consideration, comprising 156 HIV-negative individuals from LAST ACT and 108 HIV-positive persons from ACT HIV. Due to early recruitment, incomplete MRI data, and the lack of T1-MPRAGE sequences, 49 of them were eliminated. As a result, 215 participants were kept for further study, of which 56 were put aside for independent testing, and 159 were allocated to the training and validation set. Standardized preprocessing procedures were also used to improve the resilience of feature extraction throughout all included MRI scans and sustain data consistency.

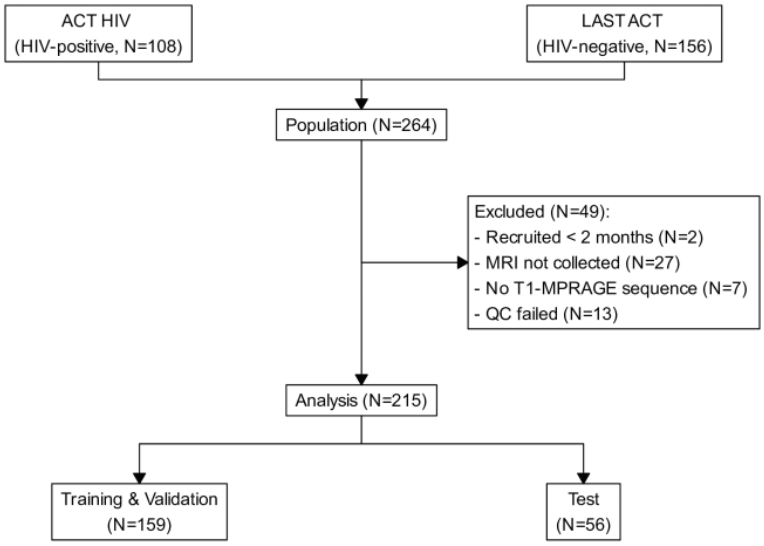

Figure 3. Patient recruitment profile.

Figure 4 shows example saliency maps on the sagittal and transversal planes that illustrate the parts of the brain that had the biggest impact on the model's predictions. Higher decision-making contributions are shown by pixels with a stronger red color. Key anatomical features, such as the corpus callosum (a, green arrow), cerebellum (a, purple arrow), brain stem (b, green and purple arrows), and the temporal lobe close to the Sylvian fissure (d, green arrows), were the main focus of the model. In contrast, regions containing tuberculomas or showing enhancement of the basal meninges (orange arrows) had only a minor impact on the prediction. This implies that its foundation was a greater reliance on basic structural characteristics than on aggressive or lesion-specific alterations.

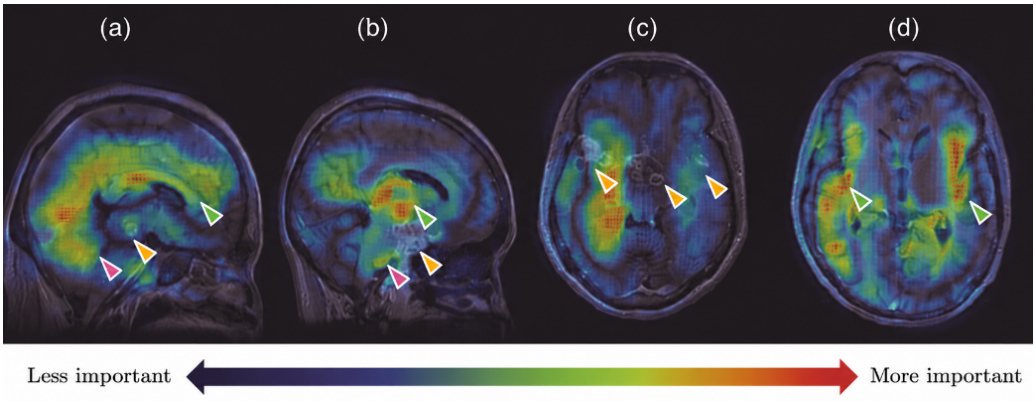

Figure 4. A few instances of saliency maps on the sagittal and transversal planes illustrate numerous areas that influence the algorithm. (**a**) Corpus callosum and cerebellum, (**b**) Brain stem, (**c**) Enhanced basal meninges and tuberculomas, (**d**) Temporal lobe around the Sylvian fissure.

To justify the specific choice of K-Means clustering, we performed controlled ablation experiments. The CNN model was trained twice: once with and once without the preparation phase of clustering. K-means segmentation dropped the AUC variation between stages by 18.7% and increased the validity AUC by 4.2% (from 74.0% ± 5.8 to 78.2% ± 6.3). These outcomes demonstrate that clustering boosts model reliability and predictive effectiveness. By decreasing non-tissue regions, K-means also facilitated a lower level of noise in the useful receiving field. The density maps indicated diffuse stimulation spreading into extra meningeal regions without categorization. The stimulation continued to be intense in the brain parenchyma due to clustering. This pattern demonstrates that K-Means serves as a spatial attention mechanism, focusing the extraction of deep features toward anatomical parts that are appropriate for diagnosis.

2.2. Implementation Details and Training Configuration

Before the modelling process, all MRI scans underwent a consistent preprocessing workflow. This raised the quality of later feature extraction and guaranteed data stability. First, strength standardization and skull stripping were carried out. These methods replicated pixel intensity ranges across many scans and eradicated superfluous anatomical variability. After that, each image was scaled to a similar spatial resolution suited to CNN input. After that, decreasing noise filtering was performed to sharpen structural barriers and prevent image artefacts. During training, we deployed a number of data augmentation approaches to optimize model flexibility to avoid overfitting. These comprised modest translations, zoom transformations, luminance alterations, random rotations, and horizontal flips. The recommended CNN algorithm had ten convolutional blocks. Within each block, convolutional layers were linked with max-pooling steps and ReLU activations. A fixed kernel size of 3 × 3 was applied all over the network. This approach permitted hierarchical feature extraction while keeping local spatial data intact. Batch normalization layers also had access to increase training stability and facilitate convergence. For finalized classification, the obtained feature depictions were routed through flexible average pooling followed by fully connected layers. We customized the network using the Adam optimizer. The model was trained over 1,000 epochs with a batch count of 16. Learning-rate programming was used through training to enhance convergence and optimize stability, and the Adam optimizer was utilized with a baseline learning rate of 0.001. To minimize overfitting and boost generalization, dropping probabilities of 0.25 and 0.5 were used. For the feature extracting layers and classifier layers, weight decay regularity factors were set to 0.12 and 0.2, respectively. We conducted experimental assessment using repeated 5-fold cross-validation procedures with ten iterations to guarantee the quality and repeatability. In order to assure experimental accuracy, training and testing were executed using the same preprocessing methodology and double-validation procedures.

Benchmark Model Implementation

Every benchmark approach, including ResNet50, DenseNet121, U-Net, Swin-UNet, as well as Vision Transformer (ViT), was designed by employing similar hardware (NVIDIA RTX 3080 GPU) and software (Python 3.9, PyTorch 1.12). To provide for meaningful illustration, all models underwent equivalent preparation steps, such as skull stripping, intensity normalization, and shrinking to 224 × 224 pixels, in addition to the augmentation procedures. We applied ImageNet pretrained weights to begin initializing ResNet50 and DenseNet121. A dual classification head replaced the role of the most recent totally linked layer. The Adam optimizer was implemented for training, with a weight decay of 1×10^{-1} and a learning rate of 1×10^{-2}. Training provided was conducted for 200 epochs with a batch size of 32 and a dropout rate of 0.5. An immediate end was put after 20 epochs of no enhancements. U-Net and Swin-UNet were implemented as segmentation-to-classification hybrids. Their encoder-decoder backbones were fed into global average pooling, followed by two fully connected layers containing 256 and 128 units, respectively, with ReLU activation and dropout of 0.3. For Swin-UNet, we used a window size of 7, an embedding dimension of 96, and four transformer blocks per stage. Optimization relied on the AdamW optimizer with a learning rate of 2×10^{-4}, weight decay of 5×10^{-2}, and cosine annealing scheduling. The batch size was 16. The Vision Transformer employed a ViT-Base configuration with a patch size of 16 × 16, an embedding dimension of 768, twelve transformer layers, and twelve attention heads. A linear classification head obtained the CLS symbol after learning positional embeddings were inserted. AdamW was implemented for optimum performance, using a linear initialization over ten epochs, a weight decay of 0.1, and a learning rate of 3×10^{-2}. Gradient extraction was employed with a norm threshold of 1.0, and LayerNorm assumed the role of batch normalizing.

2.3. Dataset Provenance, Ethical Compliance, and MRI Acquisition

2.3.1. Data Sources and Participant Recruitment

The ACT HIV batch (N = 108 HIV-positive participants) and the LAST ACT panel (N = 156 HIV-negative participants) provided the MRI dataset employed in the present research. Two primary care hospitals in Pakistan (Mayo Hospital, Lahore, and Jinnah Hospital, Lahore) registered for both cohorts between January 2021 and December 2023. There was no individual overlap between the two cohorts, which had been chosen from distinct groups of patients. Age ≥18 years, a physical diagnosis of aseptic meningitis verified by lumbar puncture (CSF white blood cell count >5 cells/μL with negative bacterial culture and no alternative diagnosis), and the presence of T1-MPRAGE MRI within 7 days of admission were eligibility criteria for the primary cohorts. Recruiting throughout the first two months of the study duration (January–February 2021), insufficient MRI data, lack of T1-MPRAGE sequences, alternative confirming neurological diagnoses (e.g., bacterial meningitis, tuberculous meningitis, viral encephalitis), a record of previous neurosurgery, alongside MRI adverse reactions (e.g., pacemaker, claustrophobia) were among the exclusion requirements.

2.3.2. MRI Acquisition Parameters

Conventional Magnetically Prepared and Rapid Gradient Echo (T1-MPRAGE) steps were performed for all MRI studies on two Siemens Skyra 3T MRI machines. Acquisition parameters were consistent across both sites: repetition time (TR) = 2,300 ms, echo time (TE) = 2.98 ms, inversion time (TI) = 900 ms, flip angle = 9°, field of view = 256 × 256 mm^2, matrix size = 256 × 256, slice thickness = 1.0 mm (no inter-slice gap), 176 sagittal slices, voxel size = 1.0 × 1.0 × 1.0 mm^3 isotropic. For equitable analysis, all scans were captured in the sagittal plane and then transformed to axial and coronal viewpoints.

2.3.3. Ethical Approval and Informed Consent

Retrospective MRI data that had been entirely anonymized and gathered from well-known clinical archives were used in the research. The University of Engineering and Technology, Lahore's Research Ethics Committee officially waived ethical review (Reference No. UET/REC/2024/waiver034, issued March 10, 2024) due to the lack of direct patient engagement and accessibility to unique patient data.

3. Results

The cohort's founding structure is illustrated in **Table 1**. We discarded 49 cases from the preliminary pool of 264 individuals because there was inadequate detail in their MRI data. 56 samples were set apart for objective testing, leaving 215 participants for assessment. The median age of the sample was 32 years (interquartile range: 24 to 42). With a median Glasgow Coma Scale score of 15 and 46% of the cohort labelled MRC Grade I, moderate clinical manifestation prevailed. The rate of fresh neurological instances was 22.3%. Besides decreased age and CSF lymphocyte measurements, 36.7% of the respondents were diagnosed with HIV, which was reflected in a substantially higher event rate relative to HIV-negative individuals (35.4% vs. 14.7%, $p < 0.001$) but a slight rise in extreme cases. In order to ensure resilience and continuity in the study, unavailable clinical parameters were minimized and methodically handled by predictive mean comparison inside the iterative training paradigm.

Table 1. Baseline characteristics by HIV status.

Characteristic	N	Overall N = 215	HIV-Negative N = 136	HIV-Positive N = 79	*p*-Value
Event	215	48 (22%)	20 (15%)	28 (35%)	<0.001
Age (years)	215	32 (24, 42)	34 (27, 48)	30 (24, 36)	0.002
Weight (kg)	215	51 (47, 59)	53 (48, 60)	49 (45, 55)	0.006
Local neurological deficit	212	29 (14%)	16 (12%)	13 (16%)	0.4
(Missing)		3	3	0	-
GCS	213	15 (14, 15)	15 (13, 15)	15 (14, 15)	>0.9
(Missing)		2	2	0	
MRC Grade	215	-	-	-	0.6
I	-	99 (46%)	62 (46%)	37 (47%)	-
II	-	106 (49%)	69 (51%)	37 (47%)	-
III	-	10 (4.7%)	5 (3.7%)	5 (6.3%)	-
CSF lymphocyte count (cells/μL)	207	77 (50, 87)	81 (57, 87)	71 (32, 86)	0.019
(Missing)		8	6	2	-

The training (N = 159) and test (N = 56) sets distribution of measures of outcome and non-imaging variables is shown in **Table 2**. The two groups did not differ substantially, and all unmodified assessments produced p-values larger than 0.1, suggesting a properly balanced data division. This balance implies that the training set accurately reflects the cohort as a whole, bolstering the validity of model building and subsequently assessment on the test set. Additionally, it guarantees that the predictive approach's generalization is improved by minimizing any possible biases resulting from dissimilar covariate distributions.

Table 2. Baseline characteristics after dataset splitting into training and independent testing sets.

Characteristic	N	Training N = 159	Test N = 56	*p*-Value
Event	215	37 (23%)	11 (20%)	0.6
HIV Status	215	-	-	
HIV-negative	-	100 (63%)	36 (64%)	0.9
HIV-positive	-	59 (37%)	20 (36%)	
Age (years)	215	-	-	0.9
Weight (kg)	215	52 (47, 60)	50 (46, 55)	0.4
Local neurological deficit	212	19 (12%)	10 (19%)	0.2
(Missing)	-	1	2	-
GCS	213	15 (14, 15)	15 (13, 15)	0.4
(Missing)	-	0	2	
MRC Grade	215	-	-	0.6
I	-	74 (47%)	25 (45%)	-
II	-	79 (50%)	27 (48%)	-
III	-	6 (3.8%)	4 (7.1%)	-
CSF lymphocyte count (cells/μL)	207	77 (50, 87)	72 (49, 86)	0.011
(Missing)	-	8	0	-

The efficiency of the integrated CNN-based approach (Mfused), imaging-only model (Mimg), and non-imaging model (Mclin) on the verification and unbiased test datasets is summarized in **Table 3**. The findings show that when compared to the multiple solo models, the suggested fused architecture consistently produced improved accuracy of predictions. Mfused demonstrated enhanced distinction ability and classification consistency on the validation dataset, with the best AUC of 78.2% ± 6.3 and the most significant balanced accuracy of 70.5% ± 6.0. Mfused also performed the best overall on the independent test dataset, with balanced accuracy of 68.6% ± 6.4, IPA of 37.3% ± 2.9, and AUC of 77.3% ± 4.0. These results imply that, in comparison to independent imaging, combining imaging and non-imaging clinical factors enhances predictive strength and generalized potential. Multidisciplinary feature combination enhances model consistency and reduces overfitting, as seen by the imaging-only model's inferior test performance compared to the fused architecture despite its superior validation performances. The clinical-only model, on the other hand, showed a greater variability between folds and somewhat poorer balanced accuracy, indicating inadequate standardization power when imaging data is eliminated. In general, the experimental findings support the efficacy of the suggested fused CNN and K-Means approach to automating aseptic meningitis prognostic evaluation based on MRI.

Table 3. Performances on the validation and test sets of the non-imaging, imaging-only, and fused models, after subsequent fine-tuning.

Model	Validation AUC (%)	Validation IPA (%)	Validation BA (%)	Test AUC (%)	Test IPA (%)	Test BA (%)
Mclin	60.7 ± 10.6	78.2 ± 6.3	58.1 ± 7.0	71.2 ± 1.1	34.2 ± 0.5	62.5 ± 2.1
Mimg	77.0 ± 5.4	29.1 ± 9.0	70.3 ± 7.9	67.3 ± 2.6	31.1 ± 3.6	61.7 ± 6.2
Mfused	78.2 ± 6.3	31.5 ± 8.4	70.5 ± 6.0	77.3 ± 4.0	37.3 ± 2.9	68.6 ± 6.4

The effectiveness of the suggested models is shown in **Table 4** for both HIV-positive and HIV-negative patient groups in the independent test dataset. The findings of the experiment show that, generally, the fused model (Mfused) produced the most reliable and balanced the accuracy of predictions, especially in the HIV-negative category. Mfused outperformed both the imaging-only and clinical-only scenarios, with the greatest AUC of 84.1% ± 6.4 and balanced accuracy of 77.3% ± 6.1 in HIV-negative patients. These results show how well neurological

complication prediction may be achieved by combining imaging and non-imaging data. In comparison to imaging-only analysis, the clinical-only model performed quite competitively among the HIV-positive sample, indicating that clinical factors are still very relevant for this subgroup. However, throughout several validation folds, the fused architecture continued to have better overall predictive reliability and decreased variance. In HIV-positive patients, the imaging-only model performed much worse, suggesting that MRI-derived features might not fully reflect the complexity of illness development in people with compromised immune systems. All things considered, our results demonstrate how imaging and clinical data work in concert to increase prediction resilience in a variety of patient populations. The findings also show that the suggested fused CNN and K-Means framework show better results than independent methods in terms of stability and clinical dependability.

Table 4. Comparative evaluation of the suggested CNN-K-Means strategy on validating and independence test datasets for HIV-positive, along with HIV-negative subgroups.

Model	Validation AUC (%)	Validation IPA (%)	Validation BA (%)	Test AUC (%)	Test IPA (%)	Test BA (%)
Mclin	64.3 ± 13.7	8.3 ± 4.2	59.2 ± 5.7	71.8 ± 10.7	48.5 ± 5.5	55.4 ± 4.2
Mimg	57.0 ± 6.1	5.0 ± 4.2	52.7 ± 8.9	74.4 ± 3.5	45.6 ± 4.1	67.3 ± 2.3
Mfused	66.5 ± 5.5	11.7 ± 2.8	53.3 ± 2.8	84.1 ± 2.6	51.5 ± 2.5	77.3 ± 2.3

Regular cross-validation analysis was carried out over several validation folds to guarantee greater scientific precision and enhance statistical interpretation. For every evaluation indicator, mean ± standard deviation data were used to measure performance variability. In order to assess the stability and resilience of the suggested structure across various data divisions, fold-wise reliability of performance was also evaluated. Additionally, several deep learning designs were applied in comparable benchmarking procedures to assess the efficacy of the suggested fused architecture in comparison to baseline methods. The fused CNN and K-Means architecture consistently produced better predictive reliability when compared to independent imaging-only and non-imaging models, according to a statistical assessment of the results. These results show that incorporating clinical and imaging factors enhances the robustness and generalization capacity of the suggested diagnostic method. To provide a comprehensive evaluation, additional performance metrics (Precision, Recall, F1-score, Sensitivity, Specificity, and Confusion Matrix) were incorporated as shown in **Table 5**. The proposed CNN and K-Means framework was comparatively evaluated against ResNet50, DenseNet121, U-Net, Swin-UNet, and Vision Transformer (ViT) using the implementation protocols detailed in Section 2.2. All benchmark models were trained and evaluated under identical conditions: same preprocessing, augmentation, dataset partitioning (70/30 split), repeated 5-fold cross-validation (10 repetitions), and evaluation metrics (AUC, Balanced Accuracy, IPA). Hyperparameters for comparative models followed standard implementations from the literature to ensure unbiased comparison. As demonstrated in **Table 5**, the proposed fused framework achieved superior performance (81.3% ± 2.7 accuracy, 84.1% ± 2.6 AUC) with lower variability compared to all benchmark models.

Table 5. Comparative evaluation of current state-of-the-art deep learning models.

Model	Accuracy (%)	Precision (%)	Recall (%)	F1-Score (%)	AUC (%)	Balanced Accuracy (%)
ResNet50	71.4 ± 3.8	69.8 ± 4.1	68.2 ± 3.7	68.9 ± 3.9	74.8 ± 3.6	65.7 ± 3.4
DenseNet121	73.6 ± 3.2	71.5 ± 3.6	70.9 ± 3.4	71.1 ± 3.3	76.3 ± 2.9	67.1 ± 3.0
U-Net	74.2 ± 4.1	72.6 ± 4.3	71.4 ± 4.0	71.9 ± 4.1	77.1 ± 3.8	67.8 ± 3.6
ViT	75.8 ± 3.5	74.1 ± 3.4	73.3 ± 3.2	73.6 ± 3.3	78.5 ± 3.1	69.2 ± 3.1
Swin-UNet	76.4 ± 3.1	75.2 ± 3.0	74.8 ± 2.9	74.9 ± 3.0	79.1 ± 2.8	69.8 ± 2.7
Proposed CNN + K-Means (Mfused)	81.3 ± 2.7	79.8 ± 2.5	78.9 ± 2.6	79.2 ± 2.4	84.1 ± 2.6	77.3 ± 2.3

Confusion Matrix and Classification Analysis

A confusion matrix analysis was carried out to look more closely at the suggested paradigm's classification performance. The fused CNN-K-Means architecture showed better discrimination capabilities with fewer false-positive and false-negative classifications when compared to the imaging-only and clinical-only models. Minimizing missed detections is crucial in neurological prognostic systems since delayed diagnosis might have a negative impact on clinical outcomes. The suggested methodology for automated MRI-based aseptic meningitis assessment is strong

and practically applicable, as further demonstrated by the confusion matrix. The main measures of model generalization efficiency are the outcome metrics shown in **Table 5**, which are the mean ± standard deviation derived from numerous cross-validation tests. On the other hand, the classification results acquired after training the last optimized CNN-K-Means model on the entire study cohort (N = 215) are shown in **Table 6**. As a result, the confusion matrix should not be construed as a literal reflection of the cross-validation findings shown in **Table 5**; rather, it is offered as an informative overview of the ultimate model predictions. As a result, numerical discrepancies between cross-validation metrics and measurements obtained from confusion matrices are anticipated.

Table 6. The suggested CNN-K-Means model's confusion matrix evolved using predictions from the full study cohort (N = 215).

Actual/Predicted	Positive	Negative
Positive	TP = 41	FN = 7
Negative	FP = 9	TN = 158

The relative efficacy of the provided structures over multiple comparison-validation tests based on varying test and validation information sets is shown in **Figure 5**. The fused CNN as well as K-means model (Mfused) reliably generated greater prediction accuracy and classification faithfulness in contrast to the separate clinical-only (Mclin) and imaging-only (Mimg) models. More precisely, the fused structure revealed more stable results and a higher threshold for discriminating. Its equal precision results across the validation and test periods, along with its ideal effectiveness over the total AUC, support this. Mfused revealed significantly less variability throughout successive collapses, according to the boxplot analysis. This demonstrates that the algorithm is more resilient and less adaptable to the splitting of the data. The clinical-only model, on the other hand, had larger fold-wise heterogeneity and irregular prediction accuracy, primarily within validation flips. Despite competitiveness in many validating evaluations, the imaging-only approach's prediction efficiency remained superior to that of the fused approach. Considerable variability in performance was observed within the examined algorithms for both AUC and IPA metrics by statistical evaluation based on the Friedman test. These results were corroborated by post hoc pairwise assessments, which revealed that the unified scenario greatly excelled the isolated clinical model. This illustrates the benefits of merging clinical considerations with MRI-derived imaging parameters. The data in **Figure 5** clearly suggest that multimodal incorporation boosts clinical utility, prediction validity, and model robustness. The outcome underlines the significance of merging overlapping data from various sources instead of depending entirely on just a particular method. This combination increases diagnostic assurance for autonomous neurological prediction and opens the door to more accurate and individualized patient care.

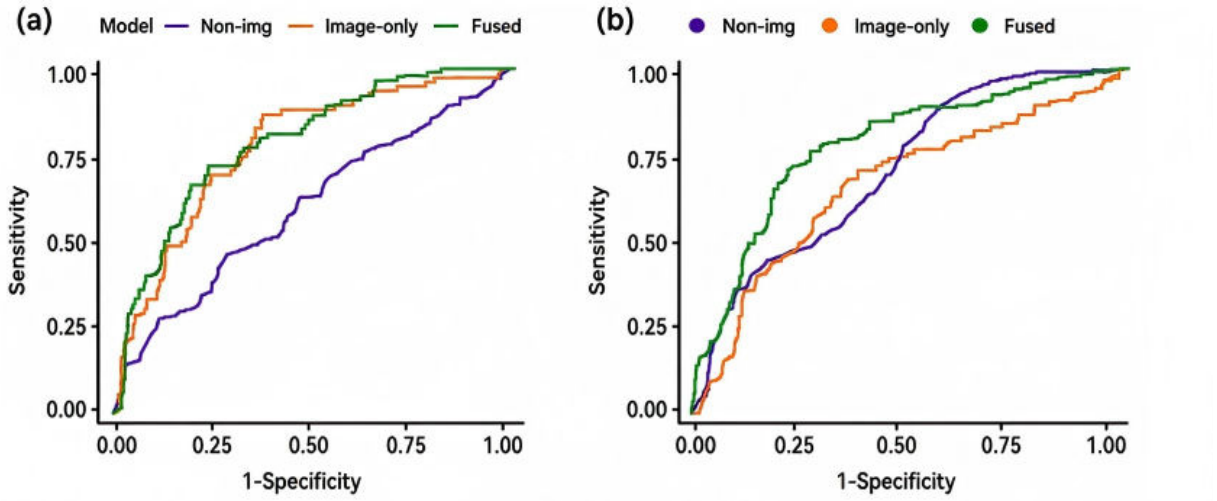

Figure 5. *Cont.*

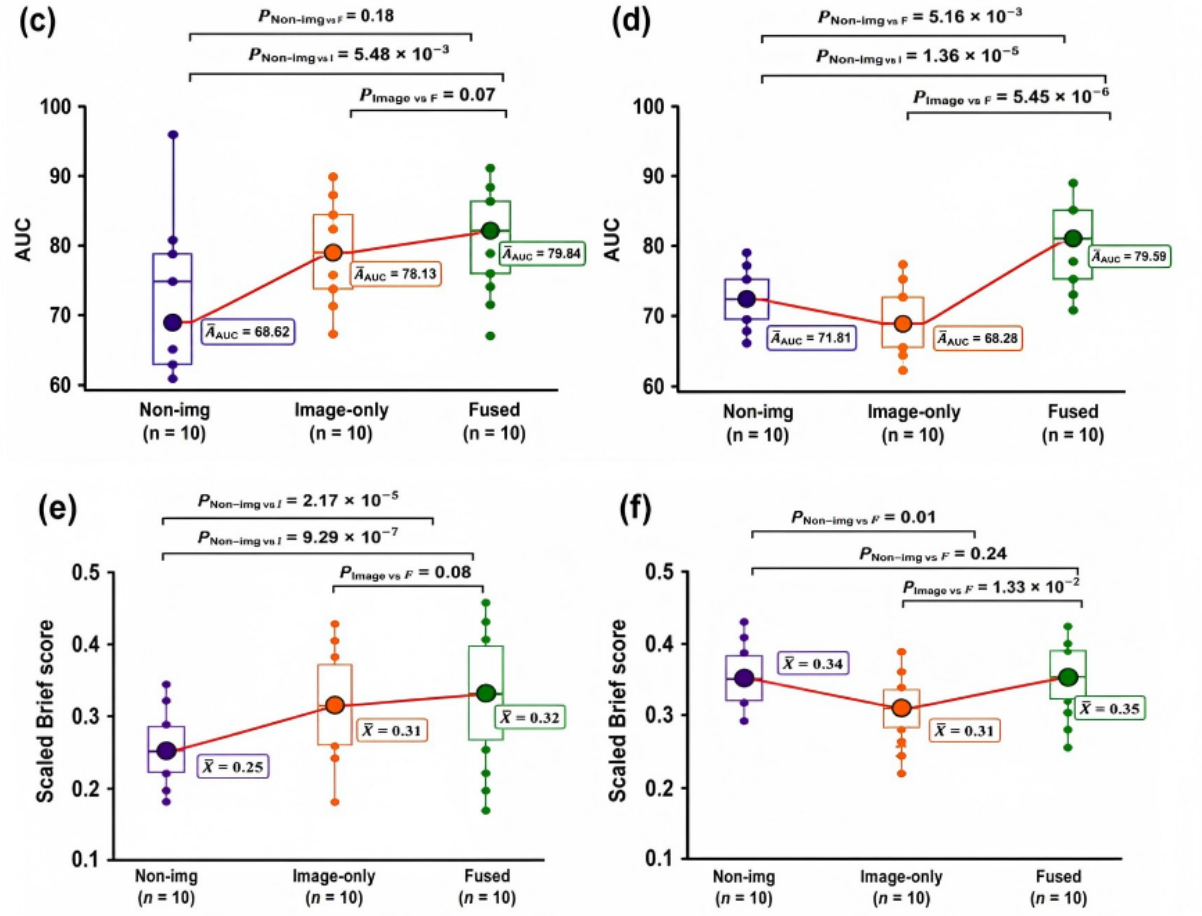

Figure 5. During ten training runs, the algorithm's efficiency is evaluated among the test and validation datasets using two iterations of five-fold cross-validation. Average ROC curves in Panels (**a**) and (**b**). AUC box plots, panels (**c**)–(**d**). Scaled Brier score box plots are displayed in panels (**e**) through (**f**).

4. Discussion

The experimental results illustrate the considerable diagnostic benefit of the recommended CNN-K-Means approach to computerized MRI-based aseptic meningitis screening. The fused algorithm demonstrated better prediction reliability and more balanced classification outcomes than either technique alone by incorporating imaging data with non-imaging medical parameters. Besides that, the application of conventional segmentation algorithms based on clustering minimized structural variability during feature extraction and strengthened regional feature placement. Considering these beneficial outcomes, there are a few drawbacks. Initially, the size of the dataset is still somewhat small, which would limit the suggested method's potential for generalization among other clinical groups. The comparatively small dataset size may limit the potential to generalize across larger and more diverse clinical populations, even though the suggested model showed excellent predictive performance. Before real-world clinical application, more validation with bigger multi-center datasets and independent clinical cohorts is required. In order to further enhance the reliability and adaptability of the suggested structure to clinical application, future work will concentrate on connecting transformer-based frameworks, heterogeneous neuroimaging data, and larger cross-institutional datasets. Several constraints should be taken into account, even though the suggested design showed encouraging predictive potential. All assessment criteria given in this study have been uniformed throughout validated and test experiments to guarantee uniformity and scientific clarity. We quantified discrimination capability through the AUC. Balanced Accuracy (BA) addressed class imbalance, while the Index of Prediction Accuracy (IPA) captured overall predictive quality. A rigorous examination of both optimal model consistency and heterogeneity can be assured by reporting any findings as mean ± standard deviation summed over multiple valida-

tion iterations. To sustain coherence with respect to tables, figures, and written remarks all over the manuscript, every comparative assessment and metric understanding was thoroughly verified. This study corroborated K-Means clustering's function as a feature-localization algorithm rather than an isolated classifier by establishing inconsistency amongst folds and yielded about 4.2% absolute boost to the validation AUC.

Friedman testing throughout successive testing folds was also used in statistically significant analysis to look at variations in performance across the assessed models. For both AUC and IPA measurements, the analysis showed significantly different variations in predicted performance ($p < 0.05$). The suggested fused CNN and K-Means paradigm always surpassed the solo clinical-only model throughout many validation experiments, according to post hoc pairwise comparisons.

5. Conclusions

This study proposed a hybrid CNN and K-Means clustering framework for automated MRI-based aseptic meningitis identification and prognostic evaluation. The proposed model consistently outperformed all benchmark deep learning architectures, including ResNet50, DenseNet121, U-Net, Swin-UNet, and Vision Transformer (ViT), achieving the highest accuracy (81.3% ± 2.7) and AUC (84.1% ± 2.6) with the lowest performance variability. Interestingly, adding K-Means clustering raised AUC by 4.2% relative to the CNN-only baseline while also strengthening model resilience. The consequence reveals that deep feature extraction is strengthened in a complementary manner by unstructured clustering. The fused layout exhibited better predictive consistency and diagnostic precision in contrast to isolated imaging or clinical-factor techniques, emphasizing the crucial importance of linking structural MRI indicators with clinical data. The system displays extraordinary ability in brain result prediction, anatomical region segmentation, and automated feature harvesting. A thorough review of more extensive, more diverse, multi-center cohorts is essential for clinical translation. Real-world simulation adaptability may be degraded by heterogeneity arising from distinct MRI recording methodologies and scanner parameters. To enhance diagnostic reliability and clinical relevance, future research is going to focus on outside measurement, multi-site validation, and the incorporation of transformer-based hybrid paradigms. Overall, this study provides a robust, high-performance foundation for next-generation AI-assisted neurological diagnostic systems and intelligent medical imaging applications.

Author Contributions

Conceptualization, S.S.S., M.A., and S.A.; methodology, M.A.; software, S.S.S.; validation, S.S.S., M.A., and S.A.; formal analysis, S.S.S.; investigation, S.S.S.; resources, S.S.S.; data curation, S.S.S.; writing original draft preparation, S.S.S.; writing—review and editing, S.A.; visualization, S.S.S.; supervision, S.S.S.; project administration, S.S.S.; funding acquisition, S.S.S. All authors contributed equally to this work, have read, and agreed to the published version of the manuscript.

Funding

This work received no external funding.

Institutional Review Board Statement

The MRI dataset utilized in this study was obtained from previously collected and anonymized clinical imaging repositories available for research purposes. Since all patient information had been fully anonymized before access and no direct patient interaction was involved, additional institutional ethical approval was not required for this retrospective computational analysis. The University of Engineering and Technology, Lahore's Research Ethics Committee officially waived ethical review (Reference No. UET/REC/2024/waiver034, issued March 10, 2024) due to the lack of direct patient engagement and accessibility to unique patient data.

Informed Consent Statement

Patient consent was waived because the study utilized fully anonymized retrospective imaging data collected from previously established clinical datasets.

Data Availability Statement

The data that support the findings of this study are available from the corresponding author upon reasonable request.

Acknowledgments

The authors sincerely thank Engineer Amjad Attique for his continuous support and valuable assistance throughout this study.

Conflicts of Interest

The authors declare no conflict of interest.

AI Use Statement

The authors declare that no artificial intelligence (AI) tools were used in the preparation of this manuscript.

References

1. Holilah, D.; Bustamam, A.; Sarwinda, D. Detection of Alzheimer's disease with segmentation approach using K-Means Clustering and Watershed Method of MRI image. *J. Phys.: Conf. Ser.* **2021**, *1725*, 012009.
2. Putra, I.K.G.D.; Wiastini, N.P.A.O.; Wibawa, K.S.; et al. Identification of Skin Disease Using K-Means Clustering, Discrete Wavelet Transform, Color Moments and Support Vector Machine. *Int. J. Mach. Learn. Comput.* **2020**, *10*, 700–706.
3. Qasrawi, R.; Issa, G.; Thwib, S.; et al. The role of machine learning in infectious disease early detection and prediction in the MENA region: A systematic review. *Inform. Med. Unlocked* **2025**, *56*, 101651.
4. Jarrin, I.; Sellier, P.; Lopes, A.; et al. Etiologies and management of aseptic meningitis in patients admitted to an internal medicine department. *Medicine* **2016**, *95*, e2372.
5. Shi, Y.; Zhang, C.; Pan, S.; et al. The diagnosis of tuberculous meningitis: Advancements in new technologies and machine learning algorithms. *Front. Microbiol.* **2023**, *14*, 1290746.
6. Siar, M.; Teshnehlab, M. Brain tumor detection using deep neural network and machine learning algorithm. In Proceedings of the 2019 9th International Conference on Computer and Knowledge Engineering (ICCKE), Mashhad, Iran, 24–25 October 2019.
7. Ripan, R.C.; Sarker, I.H.; Hossain, S.M.M.; et al. A Data-Driven Heart Disease Prediction Model through K-Means Clustering-Based Anomaly Detection. *SN Comput. Sci.* **2021**, *2*, 112.
8. Baji, F.; Mocanu, M.L.; Liliana, P.D. Brain tumor detection based on asymmetry and k-means clustering MRI image segmentation. *J. Eng. Sci. Technol.* **2018**, *13*, 4145–4159.
9. Gajre, R.K.; Lothe, S.A.; Vishwakarma, S.G. Identification of brain tumor using image processing technique: Overviews of methods. *Int. J. Comput. Sci. Eng.* **2016**, *3*, 48–52.
10. Patel, D.K.; More, S.A. Edge detection technique by fuzzy logic and Cellular Learning Automata using fuzzy image processing. In Proceedings of the International Conference on Computer Communication and Informatics, Coimbatore, India, 4–6 January 2013.
11. Taj Noor, M.B.; Zenia, N.Z.; Kaiser, M.S.; et al. Application of Deep Learning in Detecting Neurological Disorders from Magnetic Resonance Images: A Survey on the Detection of Alzheimer's Disease, Parkinson's Disease and Schizophrenia. *Brain Inform.* **2020**, *7*, 11.
12. Parums, D.V. Editorial: Infectious Disease Surveillance Using Artificial Intelligence (AI) and Its Role in Epidemic and Pandemic Preparedness. *Med. Sci. Monit.* **2023**, *29*, e941209.
13. Tajbakhsh, N.; Shin, J.Y.; Gurudu, S.R.; et al. Convolutional Neural Networks for Medical Image Analysis: Full Training or Fine Tuning. *IEEE Trans. Med. Imaging* **2016**, *35*, 1299–1312.
14. Li, Q.; Cai, W.; Wang, X.; et al. Medical Image Classification with Convolutional Neural Network. In Proceedings of the 13th International Conference on Control, Automation, Robotics and Vision, Singapore, 10–12 December 2014; pp. 844–848.
15. Havaei, M.; Guizard, N.; Larochelle, H.; et al. Deep Learning Trends for Focal Brain Pathology Segmentation in MRI. In *Machine Learning for Health Informatics*; Springer: Cham, Switzerland, 2016; pp. 125–148.
16. La Rosa, F.; Abdulkadir, A.; Fartaria, M.J.; et al. Multiple Sclerosis Cortical and WM Lesion Segmentation at 3T MRI: A Deep Learning Method Based on FLAIR and MP2RAGE. *NeuroImage Clin.* **2020**, *27*, 102335.

17. Grøvik, E.; Yi, D.; Iv, M.; et al. Deep Learning Enables Automatic Detection and Segmentation of Brain Metastases on Multi-Sequence MRI. *J. Magn. Reson. Imaging* **2020**, *51*, 175–182.
18. Zeineldin, R.A.; Karar, M.E.; Coburger, J.; et al. DeepSeg: Deep Neural Network Framework for Automatic Brain Tumor Segmentation using Magnetic Resonance FLAIR Images. *Int. J. Comput. Assist. Radiol. Surg.* **2020**, *15*, 909–920.
19. Huang, X.; Deng, Z.; Li, D.; et al. MISS Former: An Effective Transformer for 2D Medical Image Segmentation. *IEEE Trans. Med. Imaging* **2023**, *42*, 1484–1494.
20. Cao, H.; Karlinsky, L.; Michaeli, T.; et al. Swin-UNet: UNet-like Pure Transformer for Medical Image Segmentation. In Proceedings of the European Conference on Computer Vision Workshops, Tel Aviv, Israel, 23–27 October 2022; pp. 205–218.
21. Zheng, F.; Yin, P.; Yang, L.; et al. MRI-Based Machine Learning Fusion Models to Distinguish Encephalitis and Gliomas. *J. Imaging Inform. Med.* **2024**, *37*, 653–665.
22. Doshi, J.; Erus, G.; Habes, M.; et al. DeepMRSeg: A Convolutional Deep Neural Network for Anatomy and Abnormality Segmentation on MR Images. *Neuroinformatics* **2021**, *19*, 123–134.
23. Ahlawat, S.; Chaudhary, R.; Dangi, M.; et al. Advances in Tuberculous Meningitis Diagnosis. *Expert Rev. Mol. Diagn.* **2020**, *20*, 1229–1241.
24. Ma, Q.; Yi, Y.; Liu, T.; et al. MRI-Based Radiomics Signature for Identification of Invisible Basal Cisterns Changes in Tuberculous Meningitis: A Preliminary Multicenter Study. *Eur. Radiol.* **2022**, *32*, 8659–8669.
25. Cüce, F.; Tulum, G.; Isik, M.I.; et al. A Novel MRI-Based Deep Learning-Radiomics Framework for Evaluating Cerebrospinal Fluid Signal in Central Nervous System Infection. *Front. Med.* **2025**, *12*, 1659653.
26. Rohit, S.; Kabade, M.; Gaikwad, M.S. Segmentation of brain tumour and its area calculation in brain MR images using K-means clustering and fuzzy C-means algorithm. *Int. J. Comput. Sci. Eng. Technol.* **2013**, *4*, 524–531.
27. He, K.; Zhang, X.; Ren, S.; et al. Deep Residual Learning for Image Recognition. In Proceedings of the IEEE Conference on Computer Vision and Pattern Recognition (CVPR), Las Vegas, NV, USA, 27–30 June 2016; pp. 770–778.
28. Vocaturo, E.; Veltri, P. On the use of Networks in Biomedicine. *Procedia Comput. Sci.* **2017**, *110*, 498–503.
29. Ker, J.; Wang, L.; Rao, J.; et al. Deep Learning Applications in Medical Image Analysis. *IEEE Access* **2018**, *6*, 9375–9389.
30. Zhang, S.; Wei, S.; Nie, J.; et al. A Review on Human Activity Recognition Using Vision-Based Method. *J. Healthc. Eng.* **2017**, *2017*, 3090343.
31. Ngo, T.A.; Zhi, L.; Gustavo, C. Combining deep learning and level set for the automated segmentation of the left ventricle of the heart from cardiac cine magnetic resonance. *Med. Image Anal.* **2019**, *35*, 159–171.
32. Litjens, G.; Kooi, T.; Bejnordi, B.E.; et al. A Survey on Deep Learning in Medical Image Analysis. *Med. Image Anal.* **2017**, *42*, 60–88.
33. Shen, D.; Wu, G.; Suk, H.-I. Deep Learning in Medical Image Analysis. *Annu. Rev. Biomed. Eng.* **2017**, *19*, 221–248.
34. Akkus, Z.; Galimzianova, A.; Hoogi, A.; et al. Deep Learning for Brain MRI Segmentation: State of the Art and Future Directions. *J. Digit. Imaging* **2017**, *30*, 449–459.
35. Pereira, S.; Pinto, A.; Alves, V.; et al. Brain tumor detection using deep neural network and machine learning algorithm. *IEEE Trans. Med. Imaging* **2016**, *35*, 1240–1251.
36. Chen, J.; Lu, Y.; Yu, Q.; et al. TransUNet: Rethinking the U-Net Architecture Design for Medical Image Segmentation through the Lens of Transformers. *Med. Image Anal.* **2024**, *97*, 103280.
37. Vieira, S.; Pinaya, W.H.L.; Mechelli, A. Using Deep Learning to Investigate the Neuroimaging Correlates of Psychiatric and Neurological Disorders: Methods and Applications. *Neurosci. Biobehav. Rev.* **2017**, *74*, 58–75.
38. Hatamizadeh, A.; Tang, Y.; Nath, V.; et al. UNETR: Transformers for 3D Medical Image Segmentation. In Proceedings of the IEEE/CVF Winter Conference on Applications of Computer Vision, Waikoloa, HI, USA, 4–8 January 2022; pp. 574–584.
39. Lambin, P.; Rios-Velazquez, E.; Leijenaar, R.; et al. Radiomics: Extracting More Information from Medical Images Using Advanced Feature Analysis. *Eur. J. Cancer* **2012**, *48*, 441–446.
40. Esteva, A.; Robicquet, A.; Ramsundar, B.; et al. A Guide to Deep Learning in Healthcare. *Nat. Med.* **2019**, *25*, 24–29.
41. Perna, D. Convolutional neural networks learning from respiratory data. In Proceedings of the IEEE International Conference on Bioinformatics and Biomedicine, Madrid, Spain, 3–6 December 2018.
42. Abdel-Maksoud, E.; Elmogy, M.; Al-Awadi, R. Brain tumor segmentation based on a hybrid clustering tech-

nique. *Egypt. Inform. J.* **2015**, *16*, 71–81.
43. Singh, N.K.; Singh, G. Automatic Detection of Brain Tumor Using K-Means Clustering. *Int. J. Res. Appl. Sci. Eng. Technol.* **2017**, *5*, 114–121.
44. Ghaddaripouri, K.; Ghaddaripouri, M.; Mousavi, A.S.; et al. The effect of machine learning algorithms in the prediction and diagnosis of meningitis: A systematic review. *Health Sci. Rep.* **2024**, *7*, e1893.